

ALBERT-LUDWIGS-UNIVERSITÄT FREIBURG

MASTER THESIS

---

# Readout of Wavelength-shifting Optical Modules

---

*Author:*

Johannes ALT

*Supervisor:*

Prof. Dr. Horst FISCHER

February 8, 2023



*Fakultät für Mathematik und Physik*

---



## **Abstract**

todo



## **Zusammenfassung**

todo



# Contents

<b>1</b>	<b>Introduction</b>	<b>3</b>
<b>2</b>	<b>One Cell Prototype</b>	<b>7</b>
2.1	The Cell & Liquid Scintillator . . . . .	7
2.2	Wavelengthshifting Optical Module & Optical Coupling . . . . .	9
2.3	Silicon Photomultiplier . . . . .	10
2.4	The eMUSIC board . . . . .	13
2.5	The gandalf Module . . . . .	19
2.5.1	Input Mezzanine Cards . . . . .	19
2.5.2	GIMLI Mezzanine Cards . . . . .	21
2.5.3	Usage of the gandalf with Silicon Photomultipliers (SiPMs) . .	22
<b>3</b>	<b>Setup</b>	<b>24</b>
3.1	SiPM stuff . . . . .	24
3.2	dark box stuff . . . . .	25
3.3	Gandalf Stuff . . . . .	26

<b>4 Results of the DAQ Tests</b>	<b>27</b>
4.1 GANDALF Clock Frequency and ADC Test . . . . .	27
4.2 Input Offset Voltage . . . . .	29
4.3 Pole-Zero Cancellation . . . . .	35
4.4 Transimpedance and Pole-Zero Attenuation . . . . .	39
4.5 Dark Count Measurements . . . . .	42
<b>5 Data Acquisition (DAQ) performance at the Deutsches Electronen SYnchrotron (DESY) testbeam</b>	<b>45</b>
<b>6 Summary and Outlook</b>	<b>46</b>
<b>A List of acronyms</b>	<b>47</b>
<b>List of Figures</b>	<b>49</b>
<b>List of Tables</b>	<b>51</b>
<b>Bibliography</b>	<b>52</b>

# Chapter 1

## Introduction

So far, the best physical description of the universe is provided by the Standard Model (SM). However, through observations of different phenomena, which the SM can not explain, like neutrino oscillation [1] and the rotation velocity in galaxies [2], it is known that the SM can not be a complete theory [3]. Therefore different experiments are in development or are operating to search for new physics and particles outside the SM. One possible future experiment to join the search for new physics is the proposed Search for Hidden Particles (SHiP) experiment. It is an intensity frontier experiment using the 400 GeV proton beam from CERN’s Super Proton Synchrotron (SPS) and dumping it into a fixed target in order to observe rare events. SHiP is planned to be a zero background experiment to detect these rare events. It searches for long-lived heavy particles from the so-called Hidden Sector (HS), for example, heavy right-handed leptons, dark photons, and light dark matter [4].

Figure 1.1 shows the overall structure of SHiP. The 400 GeV protons get dumped into a high-density target, for example, a target out of tungsten. Through the interaction between the protons and the target, SM particles and HS particles can be produced. In order to remove the SM particles, two shieldings are used. The first one is a hadron absorber which is placed behind the target to absorb produced hadrons and electrons. Afterward, the muon shield utilizes magnetic fields to deflect the produced muons out of the beamline. So only neutrinos and HS particles remain. Behind the muon shield is a neutrino and scattering detector for secondary science



Figure 1.1: Overview of the proposed setup for the SHiP experiment. The target on the left is used as a beam dump for the SPS. Most SM particles get absorbed by the hadron absorber directly behind the target. A magnetic muon shield deflects the muon, which will not be absorbed by the hadron absorber, away from the beam line. After the muon shield is a scattering and neutrino detector, and afterward, the 50 m long decay volume in which non SM particles created at the target can decay into SM particles. Behind the decay volume, the decay spectrometer is placed. To achieve the zero background goal, the Surround Background Tagger is around the decay volume. [3]

cases. The next part is the HS decay volume. It is a 50 m long vacuum chamber in which the HS particles can decay into SM particles. The decay products then get detected in the decay spectrometer behind the HS decay volume. With the data produced by the decay spectrometer, the events can get reconstructed.

One problem for the measurement is SM particles entering the decay volume and getting falsely reconstructed as HS events in the spectrometer. An example of such a background is muons deflected by the muon shield and reflected at the walls of the facility into the decay volume, mimicking the decay products of an HS event in the spectrometer. Therefore it is crucial for the zero background requirement to detect the particles entering the decay volume and tag every event that could be caused by the entering particle as background. This task is meant to be done by the Surrounding Background Tagger (SBT). As the name suggests, it surrounds the HS decay volume, detecting particles entering it. It is currently in development and this thesis is part of the R&D effort toward it. In the following, the SBT and the principles of the different parts are described. The details of the different parts important for this thesis are presented in more detail in the next chapter.

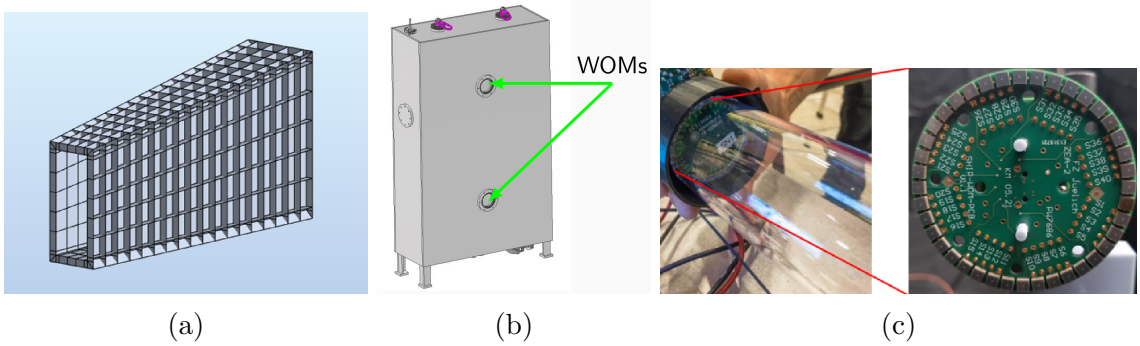


Figure 1.2: The structure of the Surrounding Background Tagger (SBT). Left is the SBT with approximately 2000 cells [1]. Then the prototype of one example cell is shown in b) [1]. The light produced by the liquid scintillator inside the cells is captured by two Wavelengthshifting Optical Modules (WOMs) per cell, an example is shown in c) [1], and then guided to an array of Silicon Photomultiplier which will detect the light.

To make the tagging of background events possible and efficient and avoid the incorrect tagging of many HS events different pieces of information need to be known about the particles entering the decay volume. These pieces of information are the energy of the entering particles, the time at which they are entering the decay volume, and the space coordinates at which they are entering. Therefore the SBT is designed as a five-dimensional tagger. It will consist of approximately 2000 cells that form the walls on the side as well as the top and bottom of the vacuum decay chamber. The structure is shown in Figure 1.2. In order to fit the overall truncated pyramid shape of the decay volume, the cells have an unsymmetric shape, an example is shown in Figure 1.2. Both of the long edges are parallel, but the shorter sides are not. The depth of the cells is 20 cm and the wall thickness is planned to be 2 cm [1]. For the detection of particles, a liquid scintillator will be filled into the cells. A particle passing through one or more cells will deposit energy in the scintillator, causing the emittance of scintillation light. The amount of emitted light is correlated to the amount of energy deposited in the scintillator. Two Wavelengthshifting Optical Modules (WOMs), PMMA tubes coated with wavelengthshifting paint, are placed in each cell to collect the scintillation light and guide it to an array of SiPMs. The signals from the SiPMs can be amplified, digitized, and further processed. Both a WOM and a SiPM array are shown in Figure 1.2.

This thesis is in the scope of the R&D of the SBT. For the R&D of the SBT, a prototype of one of the cells was built, with which important parts can be tested. Starting from the cell's material itself, a reflecting coating on the inside of the cell, the coated WOMs, and the SiPMs, to name a few. This thesis is about the readout of the WOMs of the prototype. Since the Application Specific Integrated Circuit (ASIC) meant to be used for the readout in the SBT is in development by the Forschungszentrum Jülich and not yet finished, another readout is needed for the One Cell Prototype in order to test it. The next chapter presents the One Cell Prototype with a focus on the WOM readout.

# Chapter 2

## One Cell Prototype

The work presented in this thesis is done in the framework of the One Cell Prototype. Therefore the prototype is described in more detail in this chapter. Although the important parts of the One Cell Prototype are all mentioned here, the main focus lies on the amplifier and the digitizer since these are the most relevant parts of this thesis. Firstly the cell and the liquid scintillator are shown, followed by the WOM used to capture the scintillation light, the SiPMs used for the light detection, and the optical coupling between the WOM and the SiPMs, are presented afterward. Subsequently, the amplifier and the digitizer are introduced.

### 2.1 The Cell & Liquid Scintillator

In Figure 2.1a, the One Cell Prototype is shown. It is 80 cm wide and around 120 cm high. However, the precise height depends on the position in the cell due to the asymmetric shape. The walls of the cell consist of 1 cm thick corten steel. The steel was chosen because of the rather low price tag, which is an important aspect considering the size of the SBT. A thickness of 1 cm is only half of the planned 2 cm wall thickness of the SBT design. The SBT needs such thick walls in order to withstand the vacuum on the inside. For the R&D with the One Cell Prototype, the thickness was reduced to be able to perform measurements with different wall thicknesses by adding steel plates to the outside. This is important in case the SBT



Figure 2.1: The One Cell Prototype at the DESY testbeam area a) and a PMMA vessel with a Wavelengthshifting Optical Module inserted and a SiPM board attached b). []

design changes, for example by replacing the vacuum with helium. One side of the cell has two holes with a cm radius. They have an equal distance to both side walls. The lower hole is 30 cm away from the bottom of the cell, and the upper hole is 30 cm below the top. In each of these holes, a PMMA vessel, shown in Figure 2.1b, is placed to house the two WOMs and protect their wavelengthshifting coating from the liquid scintillator. A reflective paint was applied to the inside of the cell to increase the scintillator's light yield and therefore increase the detector's efficiency.

The cell is filled with the liquid scintillator Linear Alkyl Benzene (LAB) mixed with  $2 \frac{g}{L}$  Diphenyloxazole (PPO) in order to allow decompression and compression by temperature change, an expansion vessel is mounted on top of the cell. The cell was overfilled with scintillator, in order to still being full if the temperature declines and the scintillator compresses. Gaseous nitrogen fills out the remaining volume of the expansion vessel to serve as a compressible volume.

LABs emission spectrum is shown in Figure 2.2. Most of the scintillation light has

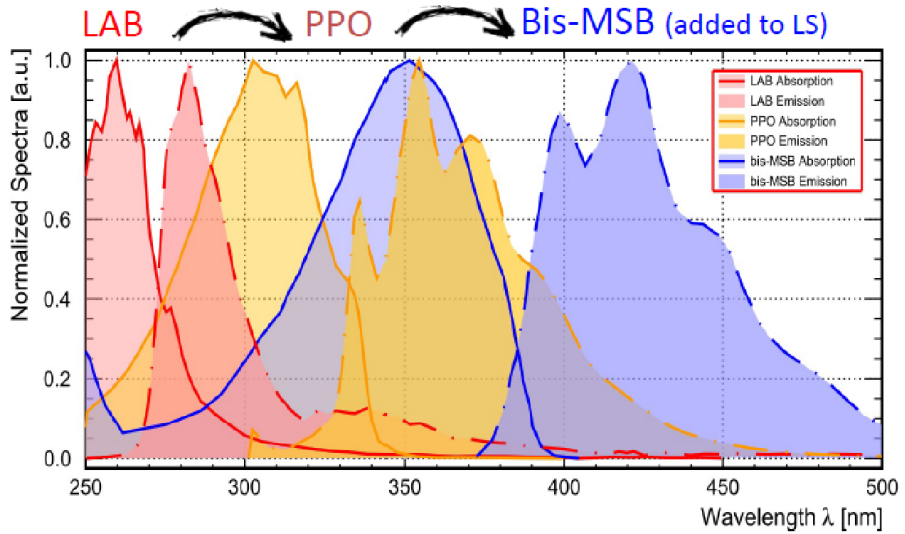


Figure 2.2: The emission spectrum of the liquid scintillator components LAB and Diphenyloxazole (PPO) and the wavelength shifter Bis-MSB. []

a wavelength of 320 nm to 360 nm. In order to capture the light and to shift the wavelength towards values for which the used SiPMs have a higher detection efficiency, WOMs are used. In the next section, these WOMs and the optical coupling between them and the SiPMs are presented.

## 2.2 Wavelengthshifting Optical Module & Optical Coupling

So-called WOMs are used to capture the scintillation light. They are PMMA cylinder walls with a 6 cm outer diameter and a 3 mm wall thickness. The design and material choice both make the cost of the light collection relatively cheap. Both the inside and outside of the PMMA cylinder are coated with the wavelength shifter Bis-MSB []. So the captured photons are shifted to a higher wavelength, for which the SiPMs used for the light detection have a higher efficiency. Figure 2.2 shows the wavelength spectrum of the wavelength-shifted light. The photons which enter the WOM are trapped there by total reflection on the walls. They can leave the WOM at its end, where an array of forty SiPMs can detect them. For a good optical coupling between the WOM and the SiPMs, either optical grease or silicon pads can be

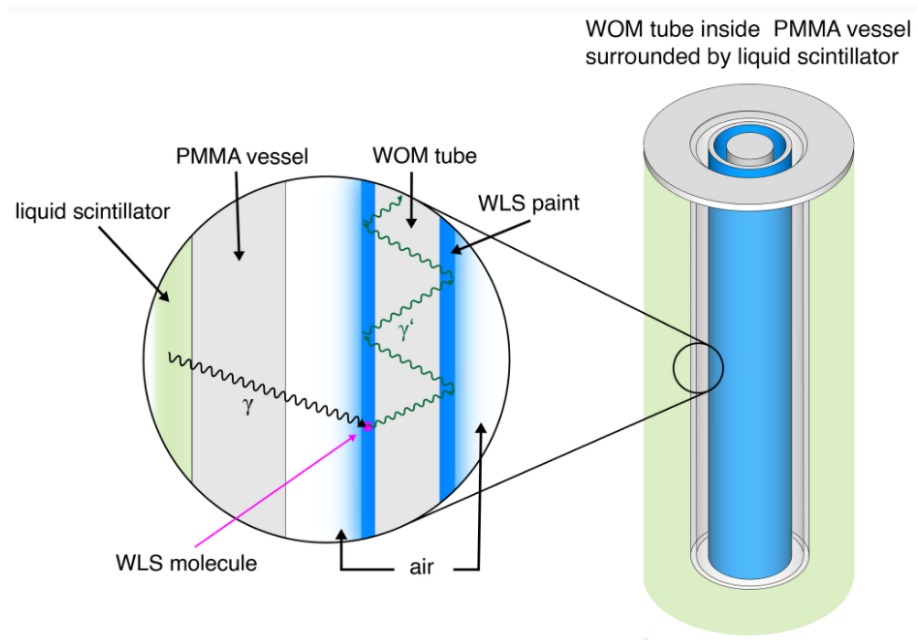


Figure 2.3: A Wavelengthshifting Optical Module (WOM) is a PMMA tube coated with the wavelength shifter Bis-MSB. If a photon in the UV range hits the WOM, its wavelength gets shifted. Afterward, in the WOM, the photon is trapped by total reflection. At the end of the WOM, the photon can be detected by a photosensor. [?, ]

used. Figure 2.3 illustrates the principle of the WOM with the wavelength shifting and capture by total reflection.

In the next part, the SiPMs, which detect the light captured by the WOMs, are presented.

## 2.3 Silicon Photomultiplier

In order to correctly identify and tag background events, the light detection of the SBT has to provide accurate timing information. Furthermore, due to the number of cells and WOMs in the SBT, it should not cost a lot per WOM. To fulfill both requirements, SiPMs were chosen as photodetectors. These photodetectors consist of up to thousands of pixels. Each pixel is a photodiode with a typical edge length between  $10\text{ }\mu\text{m}$  and  $100\text{ }\mu\text{m}$  [5]. If triggered by light, a SiPM sends out a charge

signal proportional to the number of triggered pixels. In the case that the number of incoming photons is low compared to the number of pixels, such that two photons hitting the same pixel is unlikely, the charge signal is linear to the light intensity. The charge signal possesses a fast-rising edge with a rise time of the order of tens of s [5]. Besides the excellent time resolution, SiPMs also make it possible to count the arriving photos with a sensitivity down to single photons [6].

Each pixel in the SiPM is an Single Photon Avalanche Diode (SPAD), which is a Avalanche Photodiode (APD) supplied with a voltage greater than its breakdown voltage. In the following, the principle of such an APD and SPAD are explained.

Similar to every photodiode, APD utilize, the photoelectric effect to generate an electric charge signal in response to a light signal. They consist of doped silicon. An example is shown in Figure 2.4. It has a strongly n-doped layer, followed by a strongly p-doped layer, an intrinsic, weakly p-doped layer, and another p-doped layer. By adding the intrinsic layer, the region in which the photons can be absorbed increases. If a photon gets absorbed, it generates an electron-hole pair. When a reversed bias voltage is applied, the electric field in the APD separates the *eh*-pair. In case the APD is operated in the Geiger mode, meaning the bias voltage is higher than the breakdown voltage of the APD, the electric field at the strongly doped *p*- and *n*-layer is sufficiently high, that a self-sustaining avalanche is triggered by either the electron or the hole moving through it. Then the APD is called SPAD. The macroscopic signal of a SPAD makes it possible to detect single photons. In order to stop the avalanche, a quenching resistor is connected in series to the SPAD. With an increasing current signal flowing through the quenching resistor, the voltage drop at this resistor increases, and thus the bias voltage at the SPAD decreases. When the bias voltage drops under the breakdown voltage, the avalanche is no longer self-sustaining and stops. Thus the signal amplitude of a SPAD is always similar, independent of how many photons arrive at the same moment.

In SiPMs, hundreds to thousands of SPADs are connected in parallel, each with a high-resistance quenching resistor in series. Usually, the SPAD pixels are placed in a rectangular form with an edge length of a few mm. ?? shows a picture of a SiPM and one picture of a single pixel of a SiPM. Due to the property of the SPADs that the output signal is always similar for each SPAD, the output signal of a SiPM is



Figure 2.4: Composition of an avalanche photodiode with the bias voltage  $V_B$  applied in the reverse direction. Between the contact to the ground and the strongly doped  $n^+$  layer is the quenching resistor  $R_q$  connected in series. Next to the  $n^+$  layer is a strongly doped  $p^+$  layer. In the region of these two layers is the electric field, shown in the right figure, the strongest. There, an electron or hole can initiate an avalanche. After the  $p^+$  layer is an intrinsic weakly doped  $\pi$  layer. This layer increases the sensitive volume of the diode. If an electron-hole pair is created, it gets separated by the electric field. The hole drifts towards the multiplication region and can start an avalanche. The next layer is a  $p^+$  layer, which connects to a metal connector and high voltage. The picture in the middle illustrates the number of donators  $n_D$  ad acceptors  $n_A$ , and the last picture illustrates the field strength at the different regions of the APD. []

the output signal of one SPAD multiplicated by the number of triggered SPADs. Therefore, if the number of photons arriving simultaneously at a SiPM is low enough that the probability of one SPAD being hit by two or more photons is low, one can count photons with a SiPM. This and the relatively low cost, high durability, and impassivity to magnetic fields make them a good option for photodetection for the SBT and similar detectors. However, due to the sensitivity down to single photons, also *eh*-pairs created by thermal excitation will cause signals indistinguishable from signals caused by photons. These signals are called Dark Count (DC).

An essential property of a SiPM is the gain  $G$ . It describes the number of charge carriers released in each avalanche. Due to the quenching, this parameter is well-defined [6]. It can be calculated from the applied voltage  $U_{\text{bias}}$ , the breakdown voltage  $U_{\text{bd}}$  and the capacitance  $C_d$  of a SPAD with

$$G = \frac{(V_{\text{bias}} - V_{\text{bd}}) \cdot C_d}{e}. \quad (2.1)$$

Here,  $e$  represents the charge of one electron. Usually, the gain is in the order of  $10^5$  to  $10^7$  [5]. Since the breakdown voltage of different SiPMs of the same model can differ slightly, also the gain with the same bias voltage can differ.

The next section presents the ASIC used to amplify the SiPM signals.

## 2.4 The eMUSIC board

Since the signals of the SiPMs are tiny, they need to be amplified. For this purpose, the enhanced Multiple Use SiPM IC for photodetector readout (eMUSIC) ASIC by Scientifica was chosen, and a custom Printed Circuit Board (PCB) housing the eMUSIC ASIC, from here on called eMUSIC board, was designed by the electrical engineers of the University of Freiburg. In the following first, the ASIC itself and afterward, the eMUSIC board will be presented.

**The eMUSIC ASIC** was developed by Scientifica for the readout of SiPMs. It is mainly an amplifier and a shaper, but it also offers other options like digital trigger signals if the signal crosses an adjustable threshold. The ASIC's block diagram is

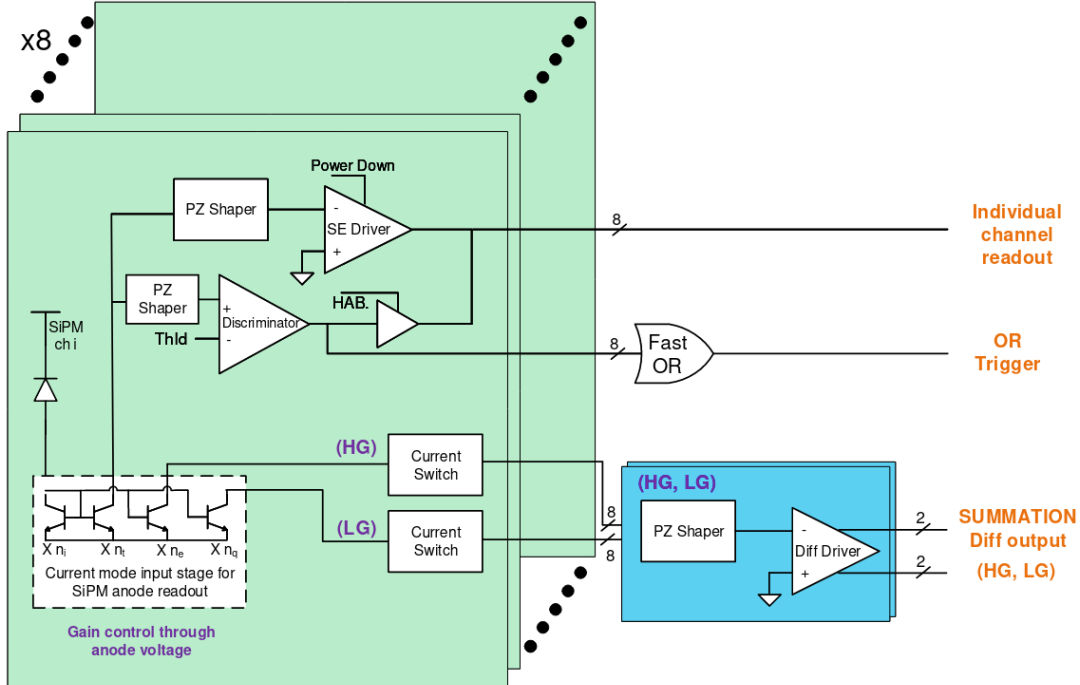


Figure 2.5: The block diagram of the eMUSIC ASIC. At the input is the current mode input stage, which can also set an offset voltage on the input to adjust the overvoltage channel by channel. The signal then gets shaped by the pole-zero cancellation shaper and amplified and can be read out for each channel as a single-ended signal. The discriminator can set a threshold to create a digital signal which can be read out channel by channel instead of the analog output signal. A fast OR output can also be used to put out a digital OR of all eight discriminator outputs. With the summation outputs, one can put out the sum of an arbitrary set of channels with two gains as differential signals. [?]

shown in Figure 2.5. It has eight input channels, each equipped with a  $\approx 1\text{V}$  anode voltage control to equalize the applied overvoltage between the different channels. Because the SiPMs deliver a charge signal, each channel has a current mode input stage. The eMUSIC ASIC was designed to have a low input transimpedance but provides the option of a high transimpedance mode with which the gain can be increased. Each individual channel has a bandwidth of 150 MHz and a pole-zero cancellation, schematics shown in Figure 2.6, with two adjustable resistors and an adjustable capacitor. It can be used to decrease the Full Width at Half Maximum (FWHM) of the output signal to below 10 ns. But a smaller width also attenuates

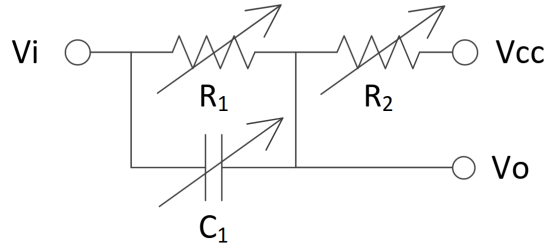


Figure 2.6: Sketch of a pole-zero cancellation with adjustable resistors and capacitor, the input voltage  $V_i$ , the output voltage  $V_o$ , and the operation voltage  $V_{cc}$ . [?]

the amplitude of the signal. The resistor has eight possible values it can be set to, and the capacitor has thirty-two different steps. Although the eMUSIC provides the option of a lower attenuation mode of the pole-zero cancellation, a compromise between smaller signal width and higher amplitude should be chosen depending on one's needs. Alternatively, the pole-zero cancellation can be disabled completely, resulting in the highest signal amplitude possible with the eMUSIC but also in the longest signal. The signal after the shaper can be put out with an analog output for each channel.

Each channel also possesses a discriminator with an adjustable threshold to create a channel-by-channel trigger signal. These logical signals can be either put out by using the individual output of the channel for the digital signal instead of the analog waveform or by using the fast OR of all channels. This fast OR allows, for example, the external triggering of the digitizer, which then digitizes the analog waveforms if the waveform of one or more channels surpasses the threshold. The dynamic range of the output for the single-ended signals is 1 V if the load on the output is  $50\Omega$  and 2 V if a high impedance load is used on the output. Using the low transimpedance mode, the gain of the single-ended output is  $180\Omega$ , and with the high transimpedance mode, it is  $480\Omega$ . Over the first half of the dynamic range, the response of the eMUSIC is linear, and over the second half, it is non-linear.

Besides the individual readout of the eight channels, the eMUSIC can sum up the signal of an arbitrary set of channels with both high and low gain and put them out via two differential outputs. The bandwidth of this summation output is 500 MHz, and the output range is 1.25 V. Depending on whether the high or low transimpedance

is used, the gain of the high gain summation is  $690\Omega$  or  $90\Omega$  and  $315\Omega$  or  $45\Omega$  for the low gain summation. The response of the summation output is linear over the dynamic range.

Besides choosing the channels for summation, also each of the eight single-ended outputs can be individually turned on and off. Another important option that can be configured is the adjustment of the output DC offset to maximize the rail-to-rail voltage swing.

The trigger threshold for the digital outputs can be set with two parameters. The first one is the bandgap voltage  $V_{bg}$  of the comparators, which can be adjusted in eight steps between 487.22 mV and 2436.8 mV. The second parameter sets the Digital to Analog Converter (DAC) value  $N_{DAC}$  for the comparators. It can be set to DAC counts from 0 to 511. The finer threshold steps  $V_{fine}$  can be calculated with

$$V_{fine} = 1637.79 \text{ mV} - N_{DAC} \cdot 3.1445 \text{ mV}. \quad (2.2)$$

With  $V_{bg}$  and of  $V_{fine}$  or  $N_{DAC}$ , the final threshold

$$V_{th} = 1.5 \cdot V_{bg} - 0.5 \cdot V_{fine} \quad (2.3)$$

$$= 1.5 \cdot V_{bg} - 0.5 \cdot (1637.79 \text{ mV} - N_{DAC} \cdot 3.1445 \text{ mV}) \quad (2.4)$$

can be calculated.

**The eMUSIC board** was designed at the University of Freiburg. A graphic of the board is shown in Figure 2.7. Its heart is the eMUSIC ASIC (U1). In order to program the ASIC, the ATmega328P-AU microchip (U4) is placed on the board. The microchip can be programmed with the XXXX software by XXXXX and the XXXXX, which is connected to the computer via USB and can be plugged into the J4 connector on the eMUSIC board. After programming the microchip, it only has to be programmed again if the reset button SW1 is pressed. Then the eMUSIC ASIC can be configured by using a TTL-to-USB adapter connected to a computer and the P3 connector, and the software of the minimusic board. The minimusic board is a commercial product using the eMUSIC ASIC. Due to the eMUSIC board being designed to work with the minimusic software, one avoids the need to write

software and also has the security that the used software was tested and is working correctly. Two functions of the minimusic software are not usable on the eMUSIC board, the calibration of the threshold and the calibration of the DC offset on the outputs. Therefore these two need to be set by the user.

The high voltage for the SiPMs can be supplied via the P2 SMA connector. On the backside of the PCB is an LSHM-150-XX.-XXX-DV-AN-XX connector located to connect the board to the SiPM board. Via this connector, the high voltage is brought to the SiPMs, and the signals are brought to the eMUSIC inputs. The eight single-ended outputs can be read out by the SMA connectors K1 to K8. The fast OR signal can be read out via the K9 connector. Both the high and low gain differential summation outputs are connected to the pins of the J6 connector.

The board also provides the possibility via the P1 connector to power the six LEDs soldered onto the SiPM boards. However, the usage of this is not advised since this will introduce interferences into the signals.

The amplified single-ended output signals then can be digitized. For this task, the gandalf module was chosen, which is described in the next section.

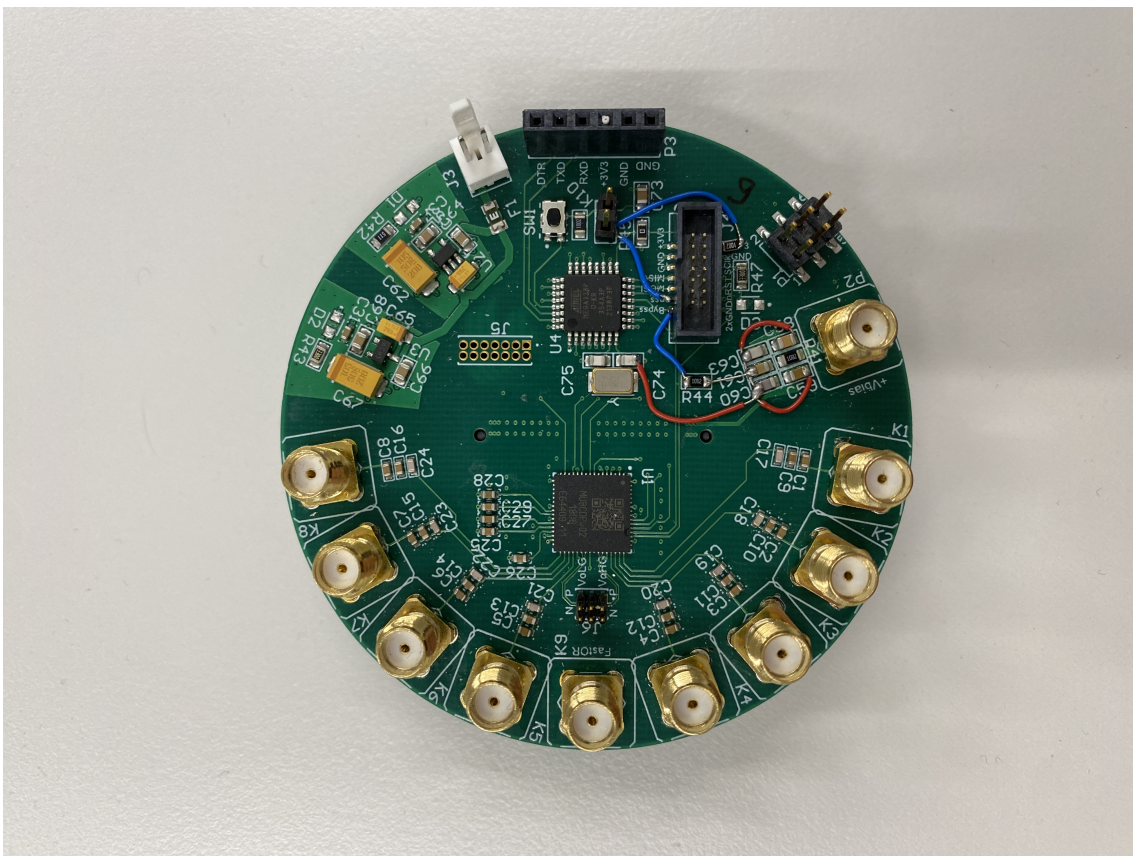


Figure 2.7: Picture of the eMUSIC board with the eMUSIC ASIC, the eight single-ended channel-by-channel SMA signal outputs, the SMA fast OR output, the differential signal output, the SMA connector for the high voltage supply of the SiPMs, and the connectors to program and power the board.

## 2.5 The gandalf Module

The amplified and shaped output signal of the eMUSIC ASIC needs to be digitized. This step is done by gandalf modules. Originally developed at the University of Freiburg for the Common Muon Proton Apparatus for Structure and Spectroscopy (COMPASS) experiment, it has a modular design to fill different roles in the experiments DAQ. Using mezzanine cards, different signal, clock, and trigger inputs can be chosen. In the following, the gandalf module will be introduced. The mezzanine cards not used in this work are therefore only mentioned but not presented in detail. An overview of a gandalf module is shown in Figure 2.8.

### 2.5.1 Input Mezzanine Cards

The gandalf module has two mezzanine card slots for input signals. For these slots, three different mezzanine cards were developed, Analoge Mezzanine Card (AMC), Digital Mezzanine Card (DMC), and Optical Mezzanine Card (OMC). First, the last two mezzanine cards are shortly presented for completeness but are not relevant to the work done in this thesis.

**The DMC** has 64 digital inputs. Using either the LVDS or the LVPECL signal standard, one can use the DSP-Field Programmable Gate Array (FPGA) logic for tasks like trigger decisions, time-to-digital conversion, or pattern generators, to name a few. By changing the direction of the input buffer on the DMC PCB, the 64 channels of the DMC can be used as outputs instead of inputs.

**The OMC** has four 3.25 Gs transceivers to receive digital information, which can be further processed by the DSP-FPGA. With this mezzanine card, the gandalf can be used, for example, to merge data or as a concentrator.

**The AMC** is designed to digitize analog input signals. For digitization, eight Analog to Digital Converter (ADC) are used. There are AMC with two different ADC available. One is the *ADS5463*, with 12 and up to 500  $\frac{\text{MS}}{\text{s}}$ , and the other is

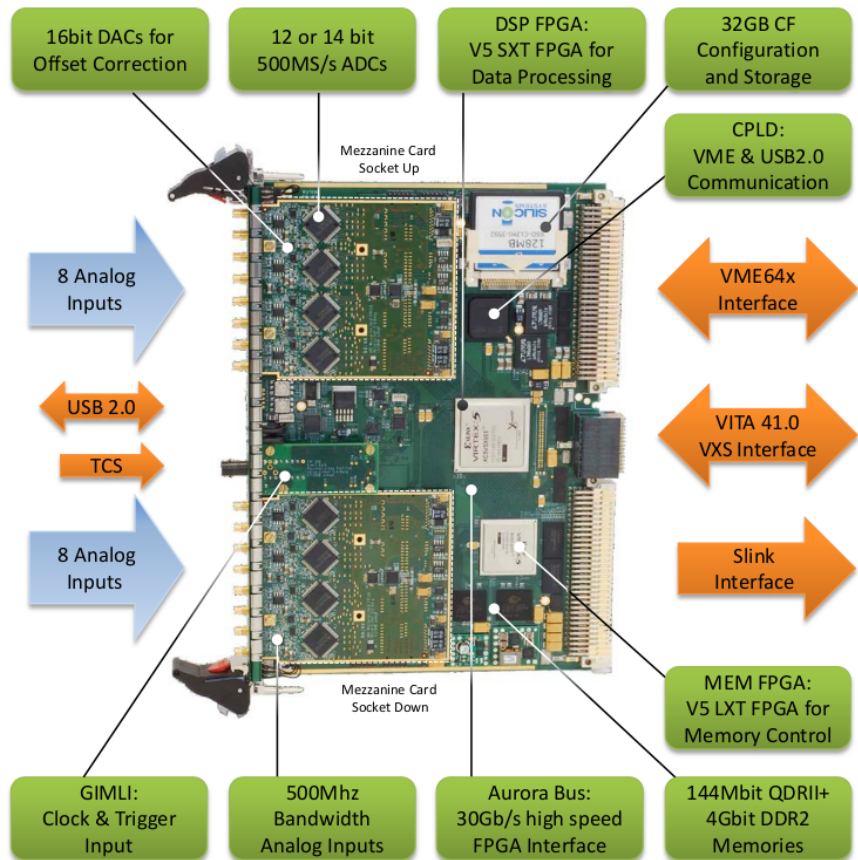


Figure 2.8: Overview of the gandalf module equipped with Analog Mezzanine Cards (AMCs) and the fiber Gimli mezzanine card for clock and trigger input. The analog waveforms are digitized by the AMCs, and the digitized data is processed by the DSP FPGA. The MEM FPGA handles the memory of the processed data, which can be transferred to a computer via the USB interface on the front of the VME or S-Link interfaces on the backplane. [?]

the *ADS5474* which samples with up to  $400 \frac{\text{MS}}{\text{s}}$  at 14. The Effective Number of Bits (ENOB) of both ADCs are 10.4 and 11.2, respectively. Each AMC has eight SMC connectors for the inputs. There are AMC operating in *normal mode*, meaning each SMC connector is connected to one ADC, resulting in eight channels with up to  $500 \frac{\text{MS}}{\text{s}}$  or  $400 \frac{\text{MS}}{\text{s}}$  per AMC. In order to increase the sampling frequency, AMCs which operate in the *interleaved mode* were built. On these AMCs, four inputs are connected to two ADCs each, and therefore every second SMC connector is a dead end. The clock signals which provide the sample tact for the two ADCs of one channel have  $180^\circ$  phase offset with respect to each other. By this, the sampling frequency is doubled to up to  $1 \frac{\text{GS}}{\text{s}}$  or  $800 \frac{\text{MS}}{\text{s}}$ , but the number of channels per AMC is reduced from eight to four. The dynamic input range of the AMC is 4.4 and can be shifted from the negative unipolar range  $-4.4 \text{ V}$  to  $0 \text{ V}$  up to the bipolar range  $-2.2 \text{ V}$  to  $2.2 \text{ V}$ . This shifting is done by an *AD5665R*, a 16 DAC. The dynamic range was chosen because in the COMPASS experiment, for which the gandalf was developed, negative voltage pulses created by Photomultiplier tubes (PMTs) needed to be digitized. However, because the used ADCs expect positive differential signals, inverting operational amplifiers are used to change the polarity of the signal. By changing the gain of the amplifiers, one can decrease the input range and therefore increase the amplitude resolution. The AMCs used in this thesis are 12 AMCs in the *interleaved mode* and a dynamic range of 2.2.

### 2.5.2 GIMLI Mezzanine Cards

The third mezzanine card slot is for the GIMLI mezzanine cards, which are responsible for the clock and external trigger signals. For this mezzanine card, three different options were developed. One GIMLI card, which takes the clock and trigger from the backplane, if one wants to use the create to distribute the signals. The fiber GIMLI has one fiber input to receive the clock and trigger via optical fiber. And the copper GIMLI, which was used for this work and is presented in the following.

The copper GIMLI, shown in Figure 2.9, provides the option to use an external or an internal clock. If only one gandalf module is used, the internal 20 MHz clock of the copper GIMLI can be used. It is provided by an onboard oven-controlled oscillator (OCXO) with a jitter of less than 2.3 ps. In case two or more gandalfs



Figure 2.9: Picture of the copper GIMLI with an internal 20 MHz clock generated by an onboard oven-controlled oscillator. With the LEMO connectors external clock and trigger NIM signals can be provided for the gandalf. [?]

are used, an external clock is required to ensure a synchronized clock on all gandalf modules. For this case, the copper GIMLI has a LEMO connector as input for an external clock with Nuclear Instrumentation Module (NIM) signal standard. Via a second LEMO connector, an external NIM trigger signal can be connected to the gandalf module.

### 2.5.3 Usage of the gandalf with SiPMs

In this work, the gandalf was used for digitizing the output signal of the eMUSIC ASIC. As mentioned above in ??, these signals have a positive polarity. But because the gandalf was designed for the digitization and processing of negative voltage pulses created by a PMT, this caused some problems. Since after the inverting operational amplifiers in the gandalf, the SiPM signals have a negative polarity, the input voltage range needs to be chosen to be bipolar and around  $-1.1\text{ V}$  to  $1.1\text{ V}$ . Also, the self-trigger of the gandalf needed to be adjusted. It functions via samples over threshold. The user can set a threshold and a number of consecutive samples which need to be over the threshold for the gandalf to trigger an event. Since after the inverting of the positive signals, the signals have a negative polarity, and the threshold needs to be set to a lower ADC value than the baseline. In addition to that, the sample over threshold condition in the gandalf firmware needed to be inverted to trigger if a number of consecutive samples were below the threshold. The new firmware with the inverted trigger condition was tested and worked as intended, with the exception of one bug. If the data rate from the gandalf to the

DAQ computer exceeds the maximum possible data rate,  $20 \frac{\text{MB}}{\text{s}}$  in the case of the USB interface, incomplete events will be written down to disk. This is most likely caused by a missing VHDL file that was not included in the new firmware and which would, in case the buffer of the gandalf is completely filled, prevent the gandalf from sending incomplete events to the computer. For the intended use of this bug should not be a problem since the data rate is expected to be way below the possible  $20 \frac{\text{MB}}{\text{s}}$ .

# Chapter 3

## Setup

### 3.1 SiPM stuff

The SiPMs mainly used in this work are the *S14160-3050HS* by the manufacturer Hamamatsu. Another SiPM model used is the SensL *J-Series 30035* manufactured by Onsemi. Some important parameters of both SiPM models are listed in Table 3.1. For this work, PCBs with each forty SiPMs of a model soldered onto it were used. A picture of one of these PCBs equiped with Hamamatsu SiPMs is shown in Figure 3.1. A breakout board can be plugged in on the back of the PCB. For this thesis the eMUSIC board was used as a breakout board, which is described in the previous chapter.

Figure 3.1: One of the PCBs with Hamamatsu SiPMs used for this work.

Table 3.1: Relevant parameters of the both used SiPM models by Hamamatsu and Onsemi. [1]

parameter	S14160-3050HS	SensL
photosensitive area / mm <sup>2</sup>	$3.0 \times 3.0$	$3.07 \times 3.07$
pixel pitch / $\mu\text{m}$	50	35
number of pixels	3000	5676
spectral response range / nm	270 to 900	200 to 900
peak sensitivity wavelength / nm	450	420
peak photon detection efficiency / %	50	
breakdown voltage / V	38	24.2 to 24.7
recommended operating voltage / V	40.7	25.2 to 30.7
variation of rec. op. voltage (typ. / max) / V	0.1 / 0.2	
gain	$2.5 \cdot 10^6$	

## 3.2 dark box stuff

To ensure a controlled environment for the measurements, the SiPMs were placed inside a dark box. The inside of the box is covered in black aluminum foil made by Thorlabs with a reflectivity in the visible wavelength spectrum below 5% [1]. An optical rail for fixing the SiPM board, a diffusor and the end of an optical fiber was placed in the box. Via the optical fiber the light of a 460 nm LED can be guided into the box. The LED is inside of another light tight box. It was build as part of the bachelor thesis of Alexander Bismark and is described there in more detail [1]. Power can be supplied to the LED via a BNC connector on the light tight box. In this thesis the Tektronix AFG was used to create voltage pulses with a width down to 4 ns. To eliminate all SiPMs equally a *ED1-C50-MD* diffuser by Thorlabs was used. For a light beam hitting the diffusor perpendicular to its surface, the light will be diffused in a circular shape with a 50° opening angle. The relative light intensity of the diffused light of a collimated 488 nm laser beam measured by Thorlabs is shown in ?? [1].

Multiple BNC, SMA, and SMC feedthroughs were installed in the dark box to supply

the SiPMs and eMUSIC board with power and to transfer the output signals of the eMUSIC out of the box to a digitizer or oscilloscope. Also a hole drilled to insert the optical fiber from the LED setup into the box and afterwards covered, to block light from entering through the hole. A power supply was used for the high voltage supply of the SiPMs. If not otherwise specified, all measurements shown in this thesis were done with a high voltage of 43 V. To control the voltage the HP multimeter was used instead of the less precise voltage display of the power supply. The eMUSIC board was powered by a 8 V power supply. For the digitization either a Generic Advanced Numerical Device for Analytic and Logic Functions (GANDALF) or the Tektronix oscilloscope was used.

?? shows a schmatic sketch of the setup inside and on the outside of the box. A picture of the setup inside the box is shown in ???. It includes the LED fiber, the diffuser, the SiPM and eMUSIC board with power and signal cables attached. In the following the setup part with the GANDALF is described.

### 3.3 Gandalf Stuff

For the operation of the One Cell Prototype sixteen channels need to be digitized, eight of each of the two WOMs. Therefore two GANDALFs are required. In order to save place and simplify the setup, the GANDALFs are not operated in a VME crate but are each in a GANDALF portable. It is a mobile case made exactly for such purposes where a whole crate is unconvienient. A picture of a GANDALF portable is shown in ???. Due to the usage of two GANDALFs an external clock is required to ensure a syncronized sampling frequency and clock for time stamps. As an external clock a copper GIMLI was chosen and used with a GIMLI testboard, shown in ???. It has two slots for GMILIs, for each one data and one clock output and a power connector to supply it with 5 V. For the purpose of an external clock, only one of these slots and the corresponding clock output is used. Via LEMO cables, the clock signal form the boards clock output pins is connected to the clock inputs of the GANDALFs.

# Chapter 4

## Results of the DAQ Tests

### 4.1 GANDALF Clock Frequency and ADC Test

Before using the GANDALF modules in the DAQ, they need to be tested. For this, two things are relevant. One of these is the sampling frequency if it corresponds to the theoretical sample frequency. The other is the test of the ADCs to see if they have dead bits or other malfunctions. To perform this test, a 150 MHz sin voltage signal was generated with an AWG and a 150 MHz filter was used. This filter ensures that the sin signal is clean and no unwanted frequencies are present. The clean sin signal was then connected to the inputs of the GANDALFs, one after another. For each input 1000 waveforms were recorded, each with 430 samples. For each channel a Fast Fourier Transform (FFT) was done for one waveform using the python3 functions `scipy.fft.rfft` and `scipy.fft.rfftfreq` to find the frequencies in the signal. ?? shows the plot with the FFT for channel 0 of the AMC 46 used with the GANDALF 23. In the plot the red line marks the peak frequency of the measured signal. The peak frequency is determined by the maxima in the frequency spectrum and the uncertainty is estimated to be half the frequency steps of the FFT. The result of the FFT is a peak frequency of  $(149.4 \pm 1.0)$  MHz. Therefore the sampling frequency of the GANDALF is as intended, which means that the external clock signal is working correctly.

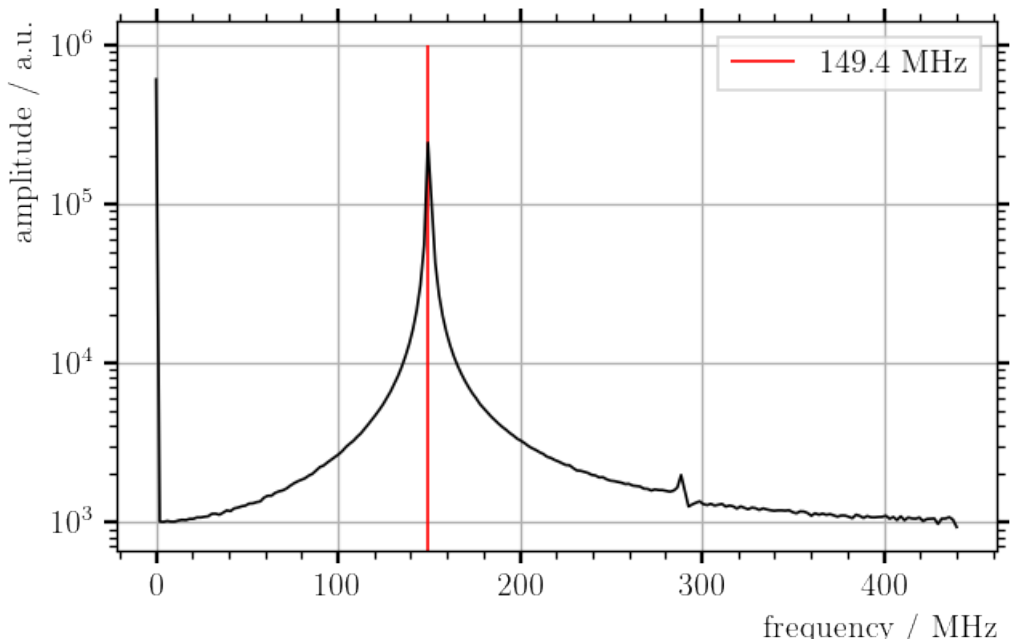


Figure 4.1: The FFT of a 150 MHz sin signal recorded with the GANDALF module 23. The peak frequency is measured is  $(149.4 \pm 1.0)$  MHz

## 4.2 Input Offset Voltage

The first measurement with the eMUSIC board is to find out the input offset voltage of the eMUSIC for different DAC values. This needs to be done to find out the exact overvoltage of the SiPMs, which influences among other things the gain of the SiPMs. In order to perform this measurement, the setup in ?? was assembled. The high voltage was set to 4.7V since it was not important for the high voltage to be over the breakdown voltage of the SiPMs. It should only be over the maximum input offset the eMUSIC can generate for the resulting voltage to be applied in reverse direction to the SiPMs. For this measurement the eMUSICs input DAC settings, which can range from 0 to 511, were set to 0. Then the voltages between the negative high voltage pole and the voltage on the cathode of the SiPMs were measured. As measurement point for the cathode voltage, the  $0\Omega$  resistor placed on the back of the SiPM board was chosen. It is shown in ?. This measurement was done for one SiPM of each SiPM group. The chosen SiPM were 1, 6, 11, 16, 21, 26, 31 and 36. After measuring the voltages, the DAC setting was increased in steps of 50 DACu until 500 DACu and at each step the measurement was repeated. In the following first the measurement results of the individual channels over all tested DAC settings are presented. Afterwards, the input offset voltages of the different channels for the same setting are compared.

As an example, the measurements of all eleven tested DAC settings done with the eMUSIC board 2 and channel 0 are shown in Figure 4.2. In the upper part of the plot, the measured voltages are plotted and for the measurements with a DAC setting between 100 DACu and 450 DACu a linear fit was performed. The first two measured voltages were not included, since they visibly do not follow the linear trend. For all channels the first to measured values are at around 1530 mV which indicates that in that DACu range the different settings do not change the offset voltage. Depending on the eMUSIC board and the channel also the last one or two measured voltages were excluded from the fit since they also do not follow the linear trend and increase to around 940 mV instead of decreasing further. The resulting slope and offset of the linear fit are

$$V_{\text{offset, fit}} = (-3.438 \pm 0.028) \frac{\text{mV}}{\text{DACu}} \cdot x + (1830 \pm 8) \text{ mV} \quad (4.1)$$

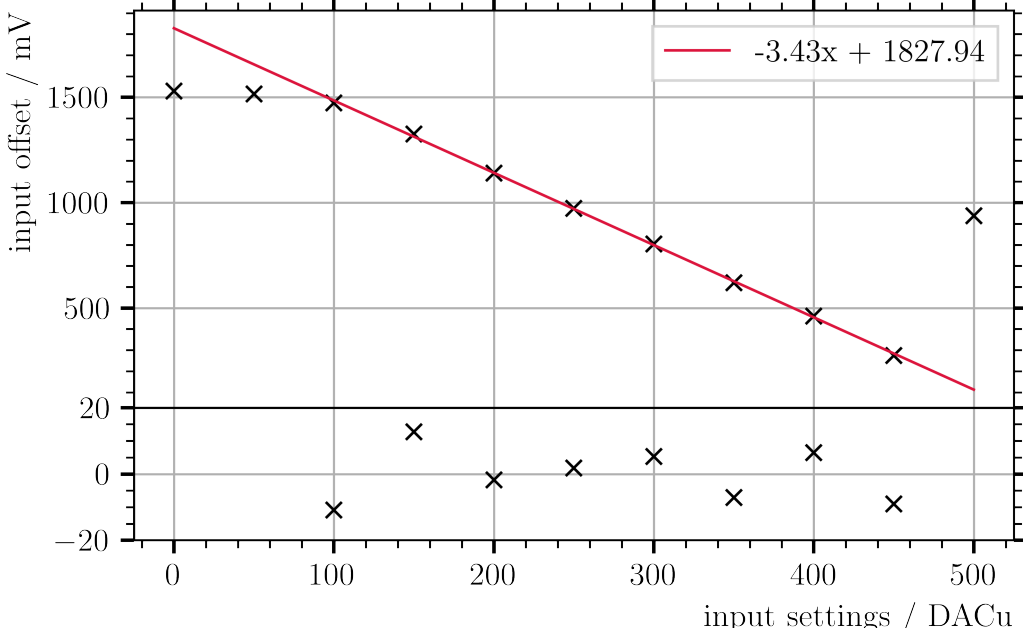


Figure 4.2: Input offset measurement for the channel 0 of the eMUSIC board 2. The input voltage was measured for input DAC settings from 0 DACu to 500 DACu in 50 DACu steps. A linear fit was performed for the measurements with DAC settings between 100 DACu and 450 DACu. The other measured voltages were excluded from the fit since they do not follow the linear trend. Below is the residual plot with a fixed y-axis window from  $-20\text{ mV}$  to  $20\text{ mV}$ .

where  $x$  is the setting of the DAC in DACu. The bottom of the plot shows the residual plot where the difference between the linear fit and the measured values is shown. The range on the y-axis is fixed to  $-20\text{ mV}$  to  $20\text{ mV}$ . From that one can see, that should be a precision of  $\pm 20\text{ mV}$  sufficient for ones used, one can use the results from the linear fit to adjust the overvoltage. In case one wants a precision in the single mV range, this is not suitable anymore. Then the DAC needs to be adjusted while measuring the voltage on the inputs of the eMUSIC ASIC. In Table 4.1 the fit results for the measurements with the eMUSIC boards 2 and 6 are listed. The DAC voltages of the channels differ to other channels on the same board as well as to the channels on the other board. Therefore the measurement of the input voltage should be done for every eMUSIC board.

To compare the differences between channels with the same DAC settings, for three

Table 4.1: The result of fitting a linear function to the input offset measurements of the eMUSIC boards 2 and 6.

eMUSIC board	channel	slope / $\frac{\text{mV}}{\text{DACu}}$	offset / mV
2	0	$-3.438 \pm 0.028$	$1830 \pm 8$
	1	$-3.405 \pm 0.015$	$1818 \pm 5$
	2	$-3.377 \pm 0.016$	$1803 \pm 5$
	3	$-3.336 \pm 0.017$	$1778 \pm 5$
	4	$-3.290 \pm 0.018$	$1764 \pm 5$
	5	$-3.316 \pm 0.020$	$1758 \pm 6$
	6	$-3.211 \pm 0.019$	$1716 \pm 6$
	7	$-3.163 \pm 0.016$	$1702 \pm 5$
6	0	$-3.472 \pm 0.019$	$1843 \pm 5$
	1	$-3.353 \pm 0.029$	$1804 \pm 9$
	2	$-3.368 \pm 0.028$	$1795 \pm 8$
	3	$-3.389 \pm 0.030$	$1801 \pm 9$
	4	$-3.260 \pm 0.050$	$1747 \pm 12$
	5	$-3.202 \pm 0.033$	$1729 \pm 10$
	6	$-3.275 \pm 0.015$	$1756 \pm 4$
	7	$-3.263 \pm 0.024$	$1749 \pm 7$

different settings the input voltage was plotted for all eight channels in Figure 4.3, Figure 4.3, and Figure 4.3. For settings at 50 DACu and below, the input offset voltage is pretty equal between the channels and only differs in the single mV range around 0 mV. A similiar behavior is seen for DAC settings at and above 500 DACu, for which the input voltage is around 940 mV and the differences between the channels is also in the single milliV range. But in the dacu range where the linear progression can be seen, the variations between the channels is larged, in some cases over 70 mV. This confirms, that the measurement of the input voltage needs to be done for all eMUSIC boards and all channels.

After these measurements were done, for the eMUSIC boards 2 and 6 the settings for which all channels have 1 V offset were determined. The resulting DAC settings and the corresponding input voltages are listed in Table 4.2. With these settings the measurement of the pole-zero cancellation and the low and high trans-impedance and pole-zero attenuation were performed. Which are presented in the following sections.

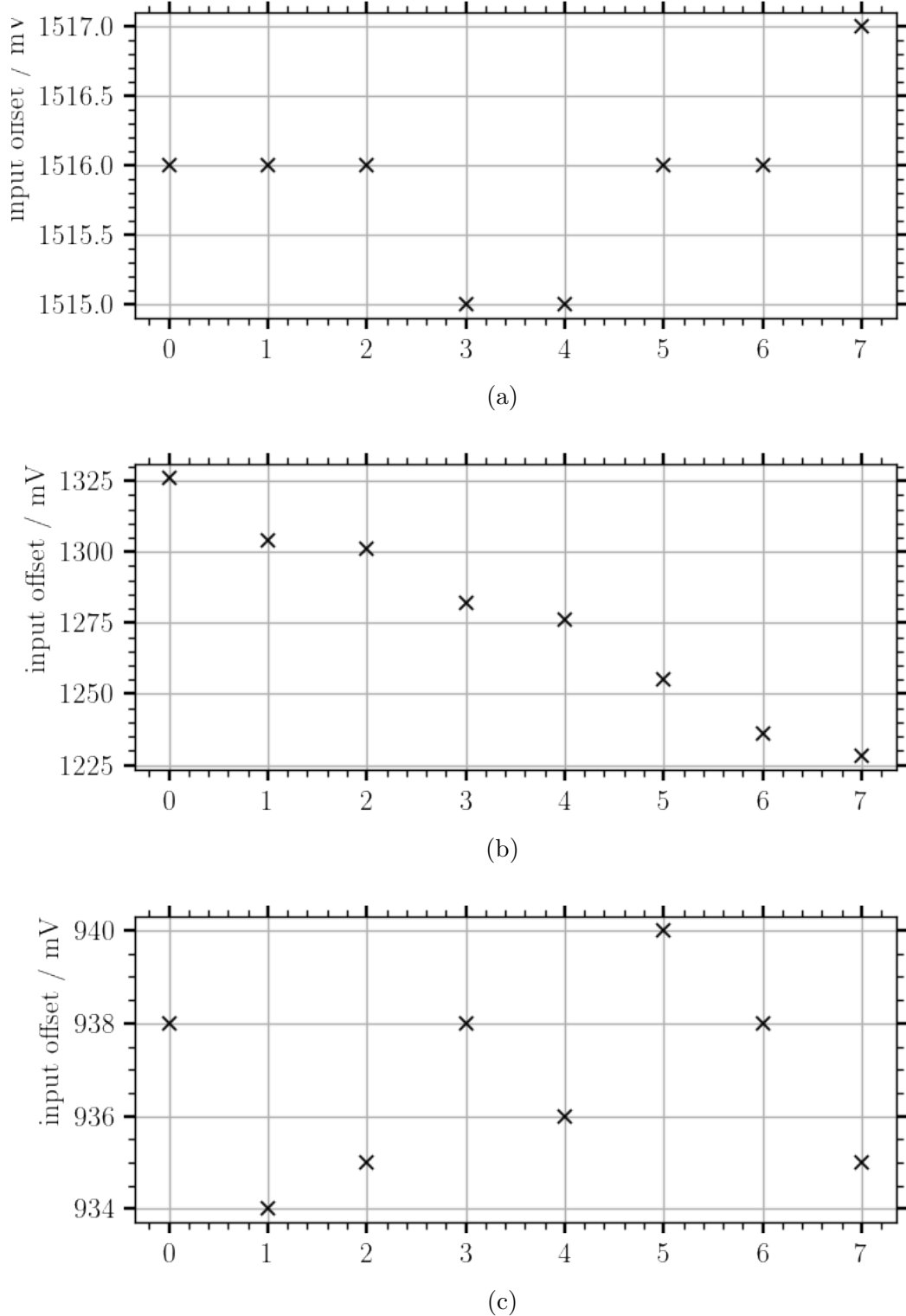


Figure 4.3: The input offset voltages of the different channels for the input DAC settings 50, 150, and 500. The shown measurements were done with the eMUSIC board 2. While the differences between the channels for the setting 50 and 500 are less than 10 mV, the maximum difference measured with the setting 150 is around 100 mV.

Table 4.2: The DAC settings for the eMUSIC boards 2 and 6 with which the input offset voltage is as near to 1 V as possible. The uncertainties of the measured voltages is estimated from the fluctuations during the measurement to be 1 mV.

eMUSIC board	channel	DAC setting / DACu	input offset / mV
2	0	0	1003
	1	50	1001
	2	100	1003
	3	150	1004
	4	200	1003
	5	250	1002
	6	300	1002
	7	350	1002
6	0	0	999
	1	50	998
	2	100	997
	3	150	1003
	4	200	1002
	5	250	995
	6	300	996
	7	350	1001

### 4.3 Pole-Zero Cancellation

In this section pole-zero cancellation shaper and its effect with different settings tested. Hereby the amplitude of the peak and the FWHM are of interest. The tests were done using the setup described in ???. The high voltage for this and all following measurements, as long as not otherwise stated, was set to 43 V. A GANDALF module was used for the digitization. The eMUSIC settings of one of these measurements are shown in ?? in the appendix. For the other measurements, the only thing changing in the settings are the pole-zero settings. Each measurement includes approximately 80 000 events, for which the mean value is shown in the plots below. The values for the amplitude and FWHM were calculated for each individual waveform and their mean values are presented here for the different measurements.

First the pole-zero cancellation was disabled to perform measurements for a reference amplitude and FWHM. In Figure 4.4 the mean of all waveforms is shown. The mean amplitude is

$$V_{amp} = (523 \pm 46) \text{ mV} \quad (4.2)$$

and the FWHM is

$$t_{FWHM} = (113 \pm 3) \text{ ns.} \quad (4.3)$$

Next the measurement with enabled pole-zero cancellation and with fixed settings for its capacitor and varying resistor values. The resistor settings were changed to all possible values, from 0 to 7, and the capacitor setting was kept at 31. Figure 4.5 presents the mean waveforms for the eight measurements. The determined amplitudes and FWHM and the corresponding decrease in respect to the values without pole-zero cancellation are listed in Table 4.3. For higher resistor values, the amplitude decreases from  $(354 \pm 30) \text{ mV}$  for the setting 0 down to  $(143 \pm 13) \text{ mV}$  for the setting 7. Also the FWHM decreases down to  $(10.2 \pm 0.6) \text{ ns}$  with higher resistor settings.

The measurements with different capacitor settings were performed with the resistor

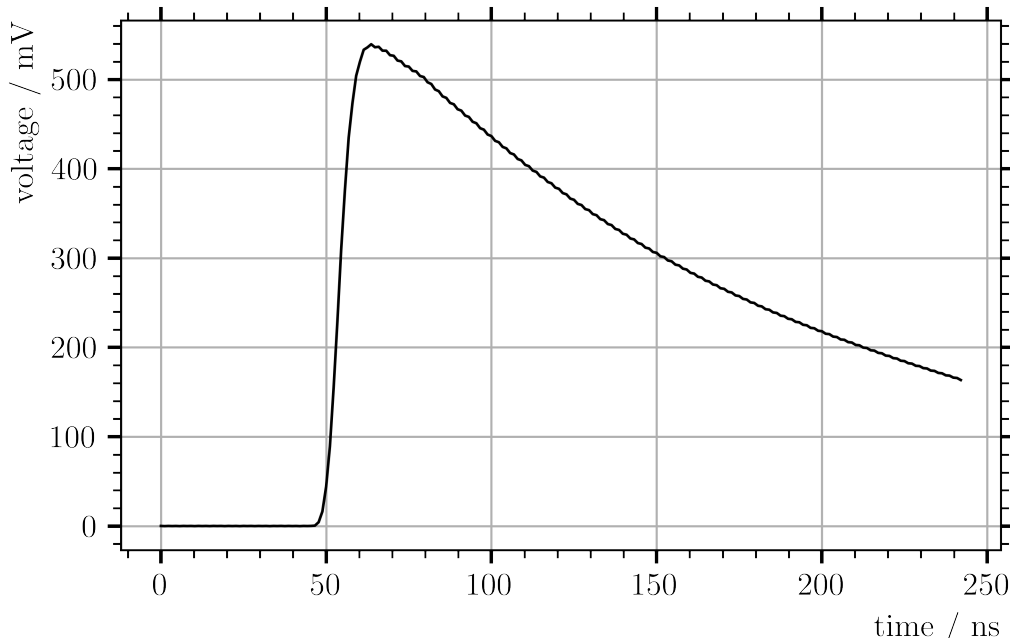


Figure 4.4: Mean waveform for a measurement without pole-zero cancellation.

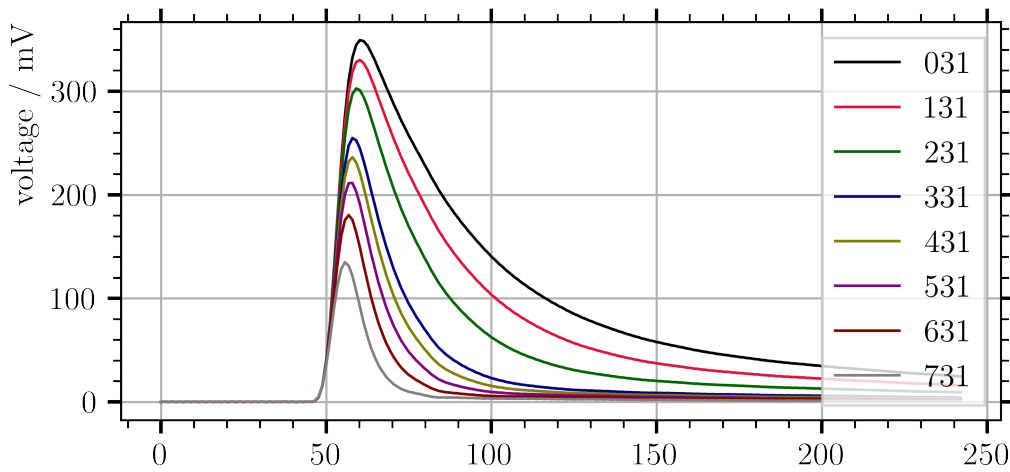


Figure 4.5: Mean waveform for different pzcanc values. The pole-zero cancellation capacitor setting was kept at 31. With increasing resistor settings the amplitude decreases and the width of the peak becomes smaller.

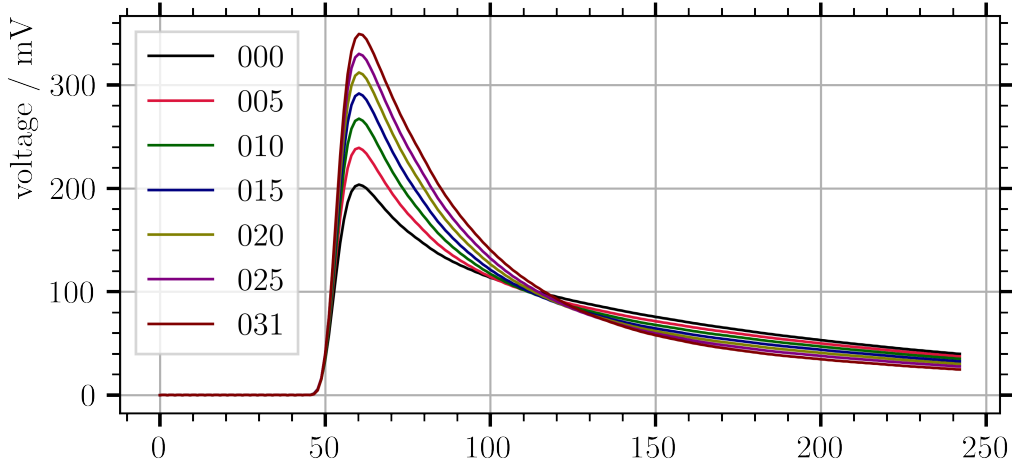


Figure 4.6: Mean waveform for different pz-cancellation capacitor values. The resistor settings were kept at 0 for all of the seven measurements.

setting of 0. For the different measurements, the capacitor settings were changed to all 32 possible values, from 0 to 31. In ?? the mean values for the maximum amplitude and the FWHM as well as the decrease compared to the values with disabled pole-zero cancellation are listed. The mean waveforms for the measurements with the capacitor settings 0, 5, 10, 15, 20, 25, and 31 are shown in Figure 4.6. Similar to the effect of the resistor, with higher capacitor settings, the FWHM decreases. For the setting 0 it is and with the maximal setting 31 it is decreased to  $(36.8 \pm 1.1)$  ns. But, opposite to the resistor setting effects, the signal amplitude increases with higher settings up to  $(354 \pm 30)$  mV. The minimal amplitude value, with the capacitor setting 0, is  $(206 \pm 17)$  mV. So by adjusting the capacitor, the amplitude can be increased by a factor of  $1.7 \pm 0.3$ .

Table 4.3: The amplitudes and FWHMs measured with different resistor and capacitor settings for the pole-zero cancellation. For each setting, around 80 000 waveforms were recorded. The listed values are the mean amplitudes and FWHMs of all corresponding waveforms.

R	C	amplitude / mV	FWHM / ns
-	-	$523 \pm 46$	$113 \pm 3$
0	31	$354 \pm 30$	$36.8 \pm 1.1$
1	31	$335 \pm 29$	$30.5 \pm 0.9$
2	31	$308 \pm 27$	$24.4 \pm 0.8$
3	31	$262 \pm 23$	$17.5 \pm 0.6$
4	31	$243 \pm 21$	$15.7 \pm 0.6$
5	31	$220 \pm 19$	$14.0 \pm 0.6$
6	31	$188 \pm 17$	$12.1 \pm 0.5$
7	31	$143 \pm 13$	$10.2 \pm 0.6$
0	0	$206 \pm 17$	$58.1 \pm 2.7$
0	5	$242 \pm 21$	$43.2 \pm 1.7$
0	10	$271 \pm 23$	$38.7 \pm 1.4$
0	15	$296 \pm 25$	$36.9 \pm 1.2$
0	20	$316 \pm 27$	$36.5 \pm 1.2$
0	25	$334 \pm 28$	$36.4 \pm 1.1$
0	31	$354 \pm 30$	$36.8 \pm 1.1$

## 4.4 Transimpedance and Pole-Zero Attenuation

After investigating the effects of the pole-zero shaper the influences between the normal and the low pole-zero attenuation settings are examined. Also the high and low transimpedance settings are investigated.

First the pole-zero attenuation was looked at. Therefore another measurement without the lower attenuation setting was performed. The pole-zero cancellation resistor setting was set to 3 and the capacitor setting was set to 31. In Figure 4.7a the mean waveforms with and without lower attenuation are presented. The peak of the waveform is not affected by the lower attenuation setting. Mainly the tail is of the waveform is increased in amplitude by using the lower attenuation. This increases the peak width, but as it can be seen in Figure 4.7a it can also prevent small overshoot of the signal.

The measurement was also done with the pole-zero settings 7 and 0 for the resistor and capacitor, respectively. The result is shown in Figure 4.7b. Here the same behavior can be observed. The peak amplitude is not influenced, only the amplitude of the tail is increased by the lower attenuation.

After the pole-zero attenuation, the high and low transimpedance settings were investigated. Therefore two measurements without pole-zero cancellation were taken with and without the high transimpedance. Both measurements consist of around 80000 waveforms. A mean waveform was calculated for both measurements and plotted in Figure 4.8. The mean amplitude of the events with high transimpedance is

$$V_{\text{high imp}} = (540 \pm 50) \text{ mV} \quad (4.4)$$

and of the events with low transimpedance the mean amplitude is

$$V_{\text{low imp}} = (185 \pm 14) \text{ mV}. \quad (4.5)$$

This results in a decrease by the factor  $0.34 \pm 0.04$  if the low transimpedance is used. The measurements were repeated with the settings 3 and 31 for the pole-zero resistor and capacitor, respectively. The mean amplitudes for these measurements

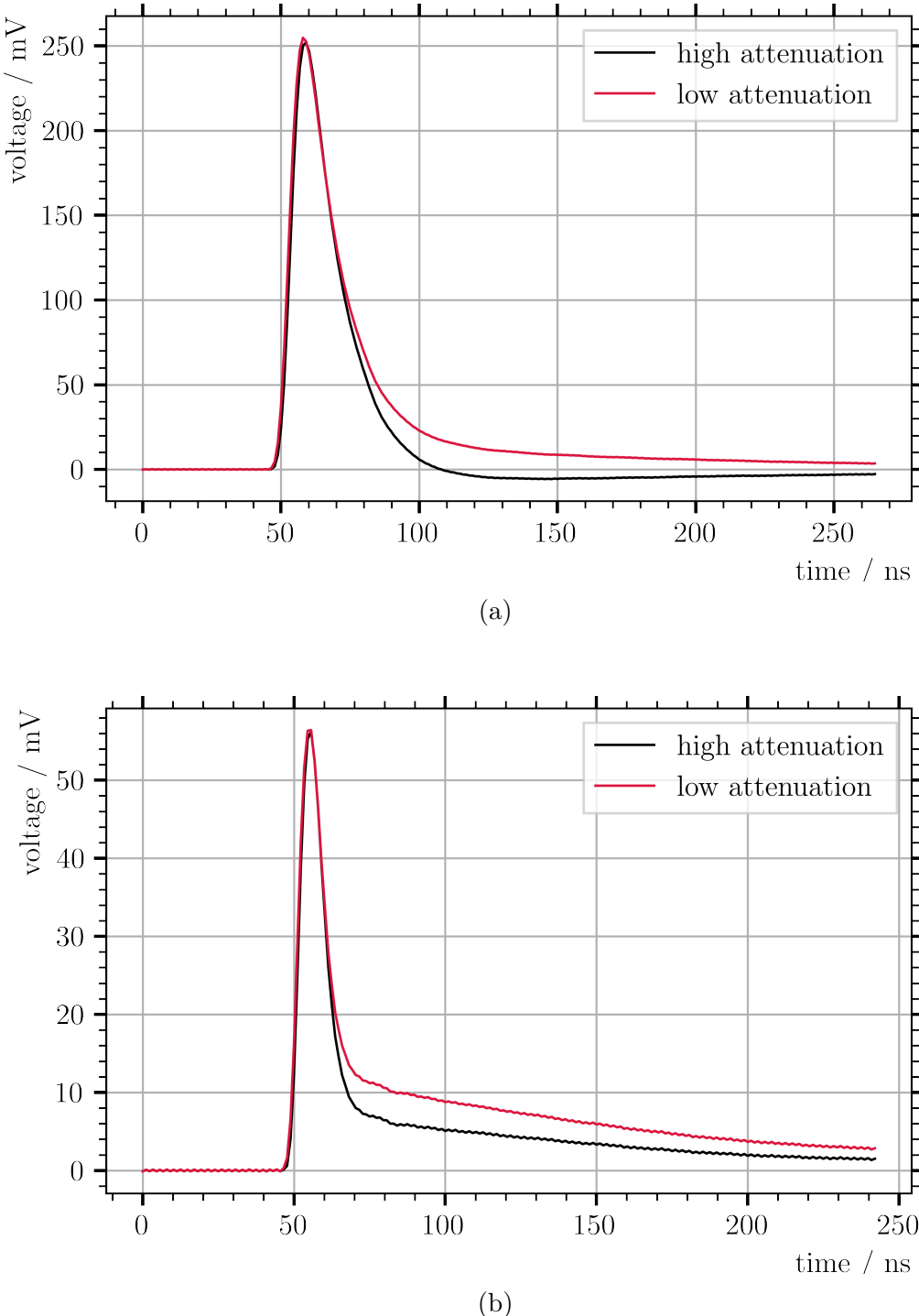


Figure 4.7: The mean waveforms of two measurements, each around 80 000 waveforms, with the pole-zero settings 7, for the resistor, and 00 for the capacitor. One measurement was done with the low attenuation option of the eMUSIC and the other was done without that option. Mostly the tail of the peaks is affected by the low attenuation option, while the peak amplitude seems to be not changed.

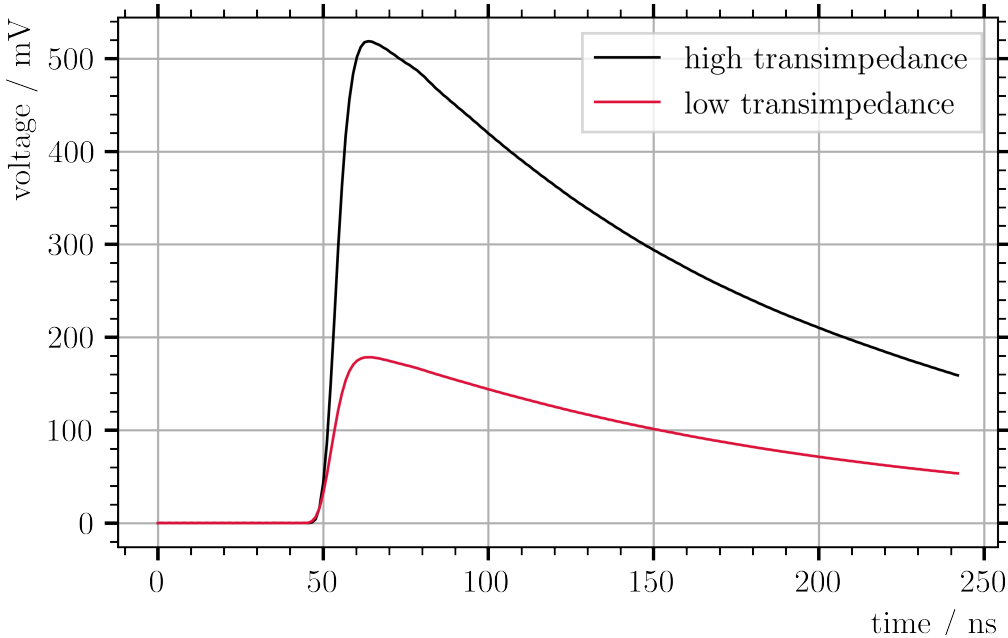


Figure 4.8: The mean waveforms of two measurements with around 80 000 waveforms each. The black waveform corresponds to a measurement done with high transimpedance and the red waveform corresponds to a measurement with low transimpedance.

are

$$V_{\text{high imp}} = (272 \pm 22) \text{ mV} \quad (4.6)$$

$$\text{and } V_{\text{low imp}} = (94 \pm 7) \text{ mV} \quad (4.7)$$

and the factor by which the signal amplitude decreases is  $0.35 \pm 0.04$ , which is also in agreement with the results of the other measurement. The plots of the mean waveforms for the measurements with pole-zero cancellation are shown in the appendix in ??.

After the, for this work, most important features of the eMUSIC are investigated, a eMUSIC board and a Hamamatsu SiPM board were used to measure dark counts. The goal of the dark count measurement was to test if dark counts could be used for calibration.

## 4.5 Dark Count Measurements

Due to their indistinguishability from signals caused by photons, the measurement of dark counts can be an easy way to calibrate the readout. To test if this is possible with the eMUSIC as amplifier, two dark count measurements were performed. For the first measurement, to maximize the amplitude, the pole-zero calibration was disabled and the high transimpedance was used. The second dark count measurement was done with enabled pole-zero calibration, low attenuation and high transimpedance. For the resistor and capacitor of the pole-zero cancellation the settings 3 and 31 were chosen, respectively. Since the amplitude of dark counts is in the lower mV range and therefore not much higher than the electronic noise, a measurement of the noise with a high voltage of 20 V was performed for comparison. To maximize the amplitude resolution, the oscilloscope was used instead of a GANDALF module. In Figure 4.9 the histograms with the integrals of a 136 ns time window around the trigger point is shown. The comparison of the dark count measurements with the noise measurement shows, that dark counts were measured. But no single photoelectron peaks can be distinguished with the measurement with pole-zero cancellation. Hence, the calibration using dark count measurements is not possible in that case. The histogram with the dark count measurement result without pole-zero cancellation is shown in Figure 4.10. Also here no single photoelectron peaks can be distinguished. Hence also without the pole-zero cancellation no calibration is possible.

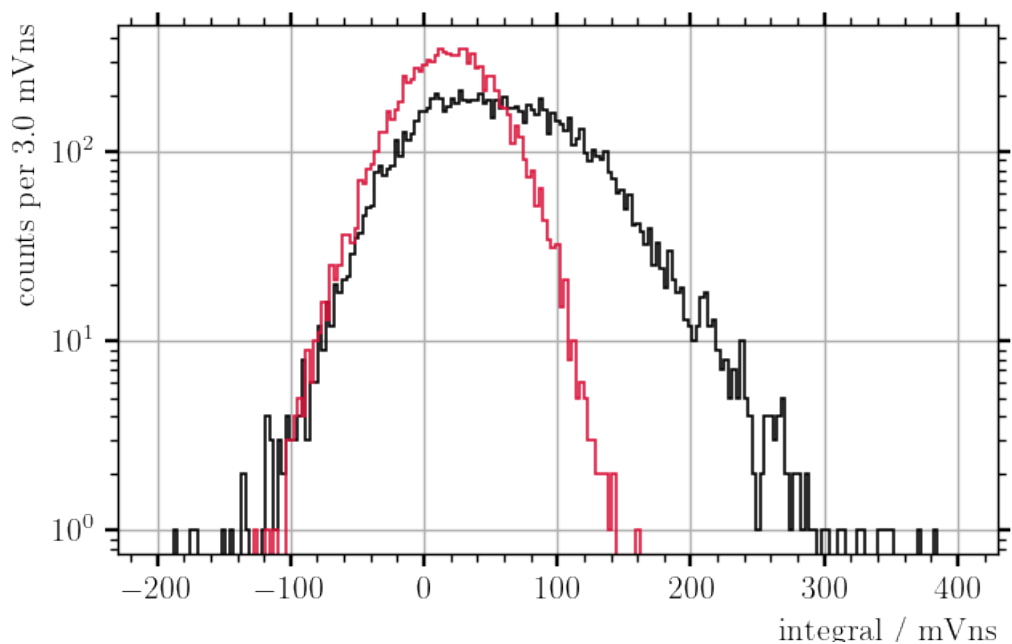


Figure 4.9: The histogram of the dark count measurements with pole-zero cancellation, and the electric noise measurement. No single photoelectron peaks can be distinguished in the dark count measurement histograms. Therefore dark count measurements cannot be used for calibration.

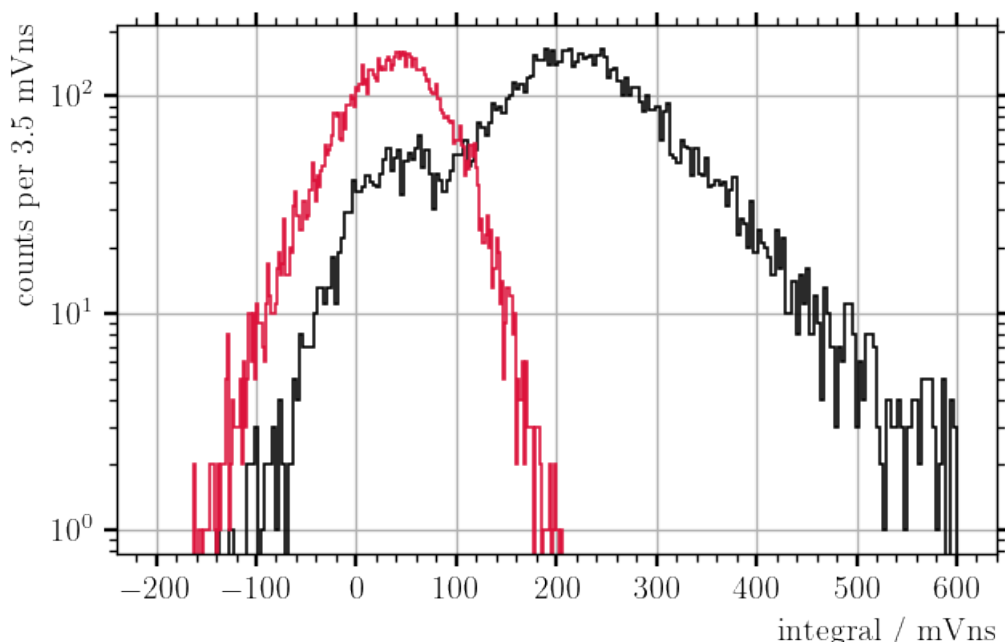


Figure 4.10: The histogram of the dark count measurements without pole-zero cancellation, and the electric noise measurement. No single photoelectron peaks can be distinguished in the dark count measurement histograms. Therefore dark count measurements cannot be used for calibration.

# **Chapter 5**

## **DAQ performance at the DESY testbeam**

After the performance of the DAQ was tested at the testbeam for one week with particles of known energy and known direction of movement, the long term performance of the one cell prototype and the DAQ needs to be investigated. For this purpose, the one cell prototype is assembled at the University of Freiburg, where it is supposed to be taking continuously data for a year. Here the majority of events will be caused by cosmic muons. By adding plastic scintillators with PMTs above and below the detector, trigger the data aquisition on a coincidence to only measure events, where the particle passed vertically through the detector. Also a way to calibrate the detector needs to be found.

# Chapter 6

## Summary and Outlook

# Appendix A

## List of acronyms

**SM** Standard Model

**LHC** Large Hadron Colider

**SHiP** Search for Hidden Particles

**SPS** Super Proton Synchrotron

**SBT** Surrounding Background Tagger

**SiPM** Silicon Photomultiplier

**PCB** Printed Circuit Board

**ASIC** Application Specific Integrated Circuit

**DAC** Digital to Analog Converter

**ADC** Analog to Digital Converter

**APD** Avalanche Photodiode

**DAQ** Data Acquisition

**WOM** Wavelengthshifting Optical Module

**SPAD** Single Photon Avalanche Diode

**DC** Dark Count

**DCR** Dark Count Rate

**FPGA** Field Programmable Gate Array

**DESY** Deutsches Electronen SYnchrotron

**eMUSIC** enhanced Multiple Use SiPM IC for photodetector readout

**PMT** Photomultiplier tube

**AMC** Analoge Mezzanine Card

**OMC** Optical Mezzanine Card

**DMC** Digital Mezzanine Card

**NIM** Nuclear Instrumentation Module

**HS** Hidden Sector

**LAB** Linear Alkyl Benzene

**FWHM** Full Width at Half Maximum

**COMPASS** Common Muon Proton Apparatus for Structure and Spectroscopy

**ENOB** Effective Number of Bits

**PPO** Diphenyloxazole

**GANDALF** Generic Advanced Numerical Device for Analytic and Logic Functions

**FFT** Fast Fourier Transform

# List of Figures

1.1	Overview of the SHiP experiment . . . . .	4
1.2	Overview of the Surrounding Background Tagger . . . . .	5
2.1	One Cell Prototype and PMMA vessel . . . . .	8
2.2	LAB emission spectrum . . . . .	9
2.3	Working principle of a WOM . . . . .	10
2.4	Illustration of a APD. . . . .	12
2.5	eMUSIC block diagram . . . . .	14
2.6	eMUSIC pole-zero cancellation . . . . .	15
2.7	eMUSIC Board . . . . .	18
2.8	Overview of the GANDALF module . . . . .	20
2.9	Copper GIMLI . . . . .	22
3.1	PCB with Hamamatsu SiPMs . . . . .	24
4.1	FFT of a 150 MHz sin signal recorded with a GANDALF module. . . . .	28
4.2	Input offset measurement for eMUSIC board 2 channel 1 . . . . .	30
4.3	Input offset voltage of all channels for differen DAC settings . . . . .	33
4.4	Mean waveform for a measurement without pole-zero cancellation. . . . .	36
4.5	Mean waveform for different pz-cancellation resistor values. . . . .	36
4.6	Mean waveform for different pz-cancellation capacitor values. . . . .	37

4.7	Plot of the low attenuation effect with two pole-zero settings. . . . .	40
4.8	Waveforms measured with low and high transimpedance . . . . .	41
4.9	Histogram of the dark count measurements with pole-zero cancellation.	43
4.10	Histogram of the dark count measurements without pole-zero cancellation. . . . .	44

# List of Tables

3.1	SiPM parameters . . . . .	25
4.1	Input offset voltages fit . . . . .	31
4.2	eMUSIC DAC settings for equal overvoltage between channels. . . . .	34
4.3	Amplitudes and FWHMs of measured signals for different PZ settings.	38

# Bibliography

- [1] SHiP - Search for Hidden Particles, <https://ship.web.cern.ch/>, June 2022
- [2] S. Alekhin et al “A facility to search for hidden particles at the CERN SPS: the SHiP physics case”, Rep. Prog. Phys. 79, Oct 2016, <https://doi.org/10.1088/0034-4885/79/12/124201>
- [3] SHiP Collaboration, “SPS Beam Dump Facility - Comprehensive Design Study”, 2020, arXiv:1912.06356
- [4] J. Kemp, “Development of a silicon photomultiplier based scintillator detector for cosmic air showers” Phd thesis, Dez 2020, RWTH Aachen
- [5] F. Acerbi, S. Gundacker, “Understanding and simulating SiPMs”, NIM-A vol. 926, p. 16-35, 2019. doi: 10.1016/j.nima.2018.11.118
- [6] Hamamatsu Photonics, MPPC, [https://www.hamamatsu.com/content/dam/hamamatsu-photonics/sites/documents/99\\_SALES\\_LIBRARY/ssd/mppc\\_kapd9005e.pdf](https://www.hamamatsu.com/content/dam/hamamatsu-photonics/sites/documents/99_SALES_LIBRARY/ssd/mppc_kapd9005e.pdf), date: 20.06.2022
- [7] Hamamatsu S14160-3050HS Datasheet, [https://www.hamamatsu.com/content/dam/hamamatsu-photonics/sites/documents/99\\_SALES\\_LIBRARY/ssd/s14160\\_s14161\\_series\\_kapd1064e.pdf](https://www.hamamatsu.com/content/dam/hamamatsu-photonics/sites/documents/99_SALES_LIBRARY/ssd/s14160_s14161_series_kapd1064e.pdf), date: 05.05.2022